Biophysical and Immunological Characterization and *In Vivo* Pharmacokinetics and Toxicology in Nonhuman Primates of the Anti-PD-1 Antibody Pembrolizumab

Beth Hutchins[1], Gary C. Starling[1], Mark A. McCoy[1], Danuta Herzyk[1], Frederique M. Poulet[1], John Dulos[1,2], Liming Liu[1], Soonmo Peter Kang[1], Laurence Fayadat-Dilman[1], Mark Hsieh[1], Christine L. Andrews[1], Gulesi Ayanoglu[1], Constance Cullen[1,3], Rene de Waal Malefyt[1,4], Robert A. Kastelein[1,4], Sabine Le Saux[1], Julie Lee[1], Sophie Li[1], Dan Malashock[1], Svetlana Sadekova[1], George Soder[1], Hans van Eenennaam[1,5], Aarron Willingham[1], Ying Yu[1], Michel Streuli[1,6], Gregory J. Carven[1,7], and Andrea van Elsas[1,8]

ABSTRACT

The programmed cell death 1 (PD-1) pathway represents a major immune checkpoint, which may be engaged by cells in the tumor microenvironment to overcome active T-cell immune surveillance. Pembrolizumab (Keytruda®, MK-3475) is a potent and highly selective humanized mAb of the IgG4/kappa isotype designed to directly block the interaction between PD-1 and its ligands, PD-L1 and PD-L2. This blockade enhances the functional activity of T cells to facilitate tumor regression and ultimately immune rejection. Pembrolizumab binds to human and cynomolgus monkey PD-1 with picomolar affinity and blocks the binding of human and cynomolgus monkey PD-1 to PD-L1 and PD-L2 with comparable potency. Pembrolizumab binds both the C′D and FG loops of PD-1. Pembrolizumab overcomes human and cynomolgus monkey PD-L1–mediated immune suppression in T-cell cultures by enhancing IL2 production following staphylococcal enterotoxin B stimulation of healthy donor and cancer patient cells, and IFNγ production in human primary tumor histoculture. *Ex vivo* and *in vitro* studies with human and primate T cells show that pembrolizumab enhances antigen-specific T-cell IFNγ and IL2 production. Pembrolizumab does not mediate FcR or complement-driven effector function against PD-1–expressing cells. Pembrolizumab displays dose-dependent clearance and half-life in cynomolgus monkey pharmacokinetic and toxicokinetic studies typical for human IgG4 antibodies. In nonhuman primate toxicology studies, no findings of toxicologic significance were observed. The preclinical data for pembrolizumab are consistent with the clinical anticancer activity and safety that has been demonstrated in human clinical trials.

Introduction

The major immune checkpoint receptor programmed cell death 1 (PD-1) is expressed on T cells following their activation, especially those that have been chronically stimulated due to viral infection or those in the tumor microenvironment (1, 2, 3). PD-1 is also expressed on NK cells in chronic infection and malignancy and on subsets of B cells and macrophages. PD-1 is a member of the immunoglobulin superfamily (4), and binds to PD-L1 and PD-L2 (5). Expression of PD-L1 increases following cell exposure to IFNγ. PD-L1 binding to PD-1 on T cells leads to recruitment of SHP-1 phosphatase to the immune synapse (6–9). The interaction of PD-1–associated SHP-1 with CD28 prevents CD28 phosphorylation and abrogates CD28-mediated costimulation. Tumor cells from a range of tissues show PD-L1 expression (10–19). PD-L1 expression in the tumor microenvironment leads to suppression of a T-cell response against the tumor (20).

Here we describe preclinical characterization of pembrolizumab (MK-3475, Keytruda®, SCH 900475), a humanized IgG4 (S228P) antibody that has been approved for treatment of cancer. Pembrolizumab is a potent inhibitor of PD-1 activity, achieved through blockade of both PD-L1 and PD-L2 by binding to a widespread structural epitope on PD-1.

Materials and Methods

Cell lines

SP2/0 cells and CHO cells expressing PD-1 were tested monthly for mycoplasma using a PCR kit. BC4-49, JY-PD-L1, and JY cells were negative for mycoplasma (last tested FEB-2018). Cell line authentication was not conducted. Peripheral blood mononuclear cells (PBMC) were collected under the Merck Research Laboratories Volunteer Donor program (MVD; Western Institutional Review Board Protocol 20121234) or clinical trial KEYNOTE-001 cohort A and with written informed consent.

Antibody generation

Wild-type BALB/c mice (Charles River Laboratories) were immunized with human PD-1 DNA and final immunization with Chinese hamster ovary cells expressing human PD-1 [CHO-hPD1 cells; Merck Sharp & Dohme Corp., a subsidiary of Merck & Co., Inc. (MSD)]. Spleen cells were isolated and subjected to positive and negative panning procedures. Clones secreting functional antibodies were identified using B-cell culture, where B cells were immortalized by

[1]Merck & Co., Inc., Kenilworth, New Jersey. [2]Galapagos, Leiden, The Netherlands. [3]Apollo Biologics Consulting, Los Angeles, California. [4]Synthekine, Inc., Menlo Park, California. [5]AIMM Therapeutics B.V., Amsterdam, The Netherlands. [6]Pionyr Immunotherapeutics, South San Francisco, California. [7]Scholar Rock, Inc., Cambridge, Massachusetts. [8]Aduro Biotech, Inc., Berkeley, California.

Note: Supplementary data for this article are available at Molecular Cancer Therapeutics Online (http://mct.aacrjournals.org/).

Corresponding Author: Beth Hutchins, Merck & Co., Inc., 213 East Grand Avenue, South San Francisco, CA 94080. Phone: 650-496-6560; Fax: 650-496-1200; E-mail: beth.hutchins@merck.com

Mol Cancer Ther 2020;19:1298–307

doi: 10.1158/1535-7163.MCT-19-0774

electrofusion to SP2/0 (ATCC) and tested in protein- and cell-based binding and ligand blockade assays, and for the ability to modulate IL2 secretion. Medical Research Council Technology (Cambridge, UK) humanized the selected antibody using complementarity-determining region grafting technology, resulting in the antibody known as pembrolizumab.

Binding to human and cynomolgus monkey PD-1, blockade of PD-L1 and PD-L2

Binding to human and cynomolgus monkey PD-1 was assessed by solid-phase interferometry and surface plasmon resonance; binding to human PD-1 was also assessed by a kinetic exclusion assay. For the solid phase interferometry format using Octet (FortéBio by Molecular Devices), recombinant human PD-1-Fc protein (MSD) or cynomolgus monkey PD-1-Fc protein (MSD) was coupled to amine-reactive biosensors per the manufacturer instructions. Association was observed by placing the sensor in wells containing 10 to 80 nmol/L antibody and monitoring for 15 minutes. Dissociation was measured after transfer into PBS and monitoring signal for 2 hours. Data sets were fit globally to a pseudo-first-order kinetics association and first-order exponential decay.

For surface plasmon resonance (Biacore; GE Healthcare Life Sciences), pembrolizumab was captured with goat antihuman IgGκ-specific antibody immobilized on a CM5 Series S sensor chip using a Biacore T100 instrument. Human or cynomolgus monkey PD-1-Fc (Sino Biologicals) was injected at various concentrations for 3 minutes, followed by a 2-hour dissociation. The on-rate (k_{on}) and off-rate (k_{off}) were empirically determined; the equilibrium dissociation constant (K_D) was determined from the k_{off} and k_{on} ($K_D = k_{off}/k_{on}$).

For the kinetic exclusion assay, a KinExA instrument (Sapidyne) was used to evaluate the solution K_D for human PD-1-Fc. Serially diluted PD-1-Fc was incubated with one of two constant concentrations of pembrolizumab, one near and one much higher than the expected K_D. After reaching equilibrium, the amount of free pembrolizumab was measured to calculate the K_D using the KinExA Pro N-curve multicurve analysis software.

Binding to human and cynomolgus monkey PD-1 and ability to block binding of PD-L1 and PD-L2 was assessed using fluorometric microvolume assay technology (FMAT). CHO-hPD-1 (MSD) or CHO-cynomolgus monkey PD-1 (CHO-cynoPD-1; MSD) and PD-L1-Fc or PD-L2-Fc fusion proteins (R&D Systems) were used. Cells were premixed with Alexa Fluor 647-labeled PD-L1-Fc or PD-L2-Fc, then mixed with unlabeled antibody at varying concentrations in FMAT plates. After reaching equilibrium, the plates were read using the FMAT system (Applied Biosystems). Total number of events detected and mean fluorescence per cell were used to calculate the IC_{50}.

Binding to CD28, CTLA-4, and ICOS used an electrochemiluminescence (ECL) immunoassay (see Supplementary Data for details). Pembrolizumab was evaluated for binding to mouse PD-1 using Octet and Biacore as described above.

Structural biology analysis of binding

Soluble PD-1 production

A gene construct encoding recombinant soluble PD-1 (sPD-1) encompassing amino acids Leu25 through Ser157 of the human PD-1 sequence with a single substitution (Cys93Ser) was expressed in *Escherichia coli*. Aliquots of guanidine hydrochloride-denatured sPD-1 were diluted into refolding buffer containing L-arginine. After concentration, monomeric sPD-1 species were isolated by size-exclusion chromatography, followed by dialysis, and ion-exchange chromatography. For nuclear magnetic resonance (NMR) experiments, ^{2}H, ^{13}C, ^{15}N isotopic-labeled sPD-1 was produced as described using *E. coli* grown in isotope-enriched media.

Production of nivolumab Fab

A Fab based on the sequence of nivolumab was expressed in 293-F cells (Life Technologies) after transfection with DNA plasmids encoding the heavy and the light Fab chains at a 1:1 ratio. Harvested supernatant was purified using Protein G (GE Healthcare) chromatography and dialyzed into 50 mmol/L HEPES, 100 mmol/L sodium chloride, pH 7.5.

Production of pembrolizumab Fab

Pembrolizumab Fab was expressed in *E. coli* and purified using Protein A chromatography (GE Healthcare). Purified Fab was formulated in PBS, 98% purity by analytical size-exclusion chromatography and >90% purity by reverse-phase chromatography.

NMR spectroscopy

NMR studies of PD-1-antibody interactions rely on the assessment of chemical shift changes to ^{15}N-labeled sPD-1 protein due to unlabeled Fab binding. Standard triple resonance techniques were first used to obtain sequence-specific assignments of ^{13}C, ^{15}N-labeled sPD-1 protein, which were supplemented from published assignments of a related construct. Next, a ^{15}N heteronuclear single quantum coherence (HSQC) data set was recorded of the ^{15}N-sPD-1/Fab complex, where only sPD-1 is ^{15}N labeled. The identification of sPD-1 residues affected by Fab binding is achieved by comparing ^{1}H and ^{15}N sPD-1 peak positions in the free and Fab complex data sets. Peak shift comparisons are made from well-resolved regions of the ^{15}N-HSQC spectrum. Mapping the NMR chemical shift perturbation data to the 3D structure of PD-1 was helpful to localize the interaction site and to set a threshold for affected residues. Data were recorded on a 500 MHz Bruker DRX500 NMR spectrometer with a high-sensitivity 5 mm cryoprobe. Peak shift analyses were made using NMRFAM-SPARKY (21) using an overlay mode to facilitate comparisons.

In vitro bioactivity

Staphylococcal enterotoxin B stimulation assays

Heparinized whole blood was obtained under written informed consent from 8 patients with prostate cancer, from 8 patients with stage IV melanoma, and from healthy volunteers; and the staphylococcal enterotoxin B (SEB) stimulation assay was performed as described previously (22).

Heparinized blood was collected from cynomolgus monkeys in the pharmacokinetic study (described below) predose (days −7 and 0) and on days 1, 7, 28, 56, and 84 postdose. Heparinized whole blood was also collected from monkeys in the 1-month toxicology study (described below), twice pretest, 24 hours after dosing on days 0 and 28, and on days 56, 98, 126, and 154 from animals assigned to the recovery period. Blood was diluted 1:10 with RPMI culture medium and preincubated for 30 to 60 minutes with pembrolizumab (at 25 to 0.00025 mg/mL) or medium, after which 1 μg/mL SEB was added and mixtures cultured for 3 days. Supernatant IL2 was measured with an ELISA Kit (eBioscience).

T-cell tetanus toxoid antigen-specific recall assay

Cryopreserved PBMCs from consenting donors revaccinated <1 year prior with tetanus toxoid (TT; Sanquin Blood Bank Nijmegen) were thawed and plated in DMEM-F12 media with 10% FBS and antibiotics as described previously (22). Cells were preincubated with antibody at concentrations up to 25 μg/mL for 30 to 60 minutes prior

to addition of 1 μg/mL TT. After 7 days, supernatants were analyzed for IFNγ by ELISA (eBioscience).

Activity on primary T-cell clone BC4-49

The human $CD4^+$, HLA-DR alloantigen-specific T-cell clone BC4-49 was generated from PBMCs of a consenting donor (Stanford Blood Center) after priming with JY cells (gift from Gilbert M. Lenoir) and cloning by limited dilution. JY-PD-L1 clone 6, a high PD-L1 cell surface-expressing puromycin-resistant clone, was generated by transfection of wild-type JY cells with a lentivirus vector pLX-301 encoding human PD-L1 (Millipore Sigma). For the activity assay, BC4-49 T cells were harvested on day 7 after antigen restimulation, washed with PBS, 2 mmol/L EDTA and resuspended in Yssel's medium (Gemini Bioproducts). The BC4-49 T cell suspension was added at 2×10^4 cells in 50 μL per well into wells containing 100 μL of serially titrated antibody. The antibody/T-cell mixture was preincubated for 1 hour. Irradiated JY and JY-PD-L1 cells were washed twice with PBS, 2 mmol/L EDTA, resuspended in Yssel's medium, and filtered. JY or JY-PD-L1 cell suspension (1×10^4 cells per well) was added to the preincubated antibody/T-cell mixtures, using a BC4-49 T cell to JY cell ratio of 2:1. After 3 days, supernatants were analyzed for IFNγ using the Human IFNγ Quantikine ELISA Kit (R&D Systems). See Supplementary Data for additional details.

Primary tumor cell culture assay

Fresh non–small cell lung cancer (NSCLC) tumor tissues were collected and shipped overnight in AQIX media (AQIX) by collection providers (Folio Biosciences, Bio-Options, and Boston Biosource). Single cells were dissociated from tumors by fine cutting with a scalpel, followed by a 30-minute incubation at 37°C in DMEM with 100 mg/mL collagenase type I, and 10,000 U/mL DNase I. Digested samples were triturated, filtered through a 70 μm strainer, and washed in DMEM complete medium. A total 0.1×10^6 tumor cells per well were stimulated with 10 ng/mL soluble anti-CD3 antibody (BioLegend, clone OKT3) in the presence of pembrolizumab or isotype control antibody. On day 7 supernatants were assayed for IFNγ using a human IFNγ Kit (Meso Scale Discovery).

Evaluation of cytokine release in human whole blood and PBMCs

PBMC cytokine release assays were conducted with plate-bound antibody using blood from eight healthy human donors (MVD). An *in vitro* whole blood assay using blood from eight healthy human donors (MVD) was also conducted with pembrolizumab in solution. Controls included known stimulatory antibodies anti-CD3 (OKT3 analog; eBioscience) and anti-CD28 (MSD TGN1412 analog), and trastuzumab. Induction of IFNγ, IL10, IL12 p70, IL1β, IL2, IL6, IL8, and TNFα was assessed by multiplex immunoassays (Meso Scale Discovery). See Supplementary Data for additional details.

Assays for antibody-dependent cell-mediated and complement-dependent cytotoxicity

Activated human PBMCs were used as effector cells and activated human CD4+ T cells from the same donor (MVD) were used as target cells for the antibody-dependent cell-mediated cytotoxicity (ADCC) assays. The ADCC assays were conducted according to the method used to assess nivolumab (23). Activated $CD4^+$ T cells were used as target cells, and human serum complement as effector molecules in the complement-dependent cytotoxicity (CDC) assays. The same activated human $CD4^+$ T cells were used as target cells in both the ADCC and CDC assays. Saturation of PD-1 on activated target human $CD4^+$ T cells by pembrolizumab was confirmed by flow cytometry. See Supplementary Data for additional details.

Ex vivo analysis of antigen-specific T-cell recall response to viral antigens

The effect of treatment with pembrolizumab on overall T-cell responses to viral infection was assessed *ex vivo* for clinical trial KEYNOTE-001 cohort A patients with solid tumors using an IFNγ ELISPOT assay (Cellular Technology Ltd.). KEYNOTE-001 was conducted in accordance with recognized ethical guidelines and approved by an institutional review board. PBMCs from 17 patients were collected before and after treatment with pembrolizumab (days 3, 8, 15, and 22; and cycle 2, day 1 preinfusion time points) under written informed consent and stimulated with a pool of peptides of Epstein–Barr virus, cytomegalovirus, and influenza virus restricted to MHC class I molecules (CEF-32; Cellular Technology Ltd.; Panatecs). Samples were analyzed using an IFNγ ELISPOT assay. See Supplementary Data for additional details.

Pharmacokinetics and toxicologic evaluation of pembrolizumab in cynomolgus monkeys

In a single-dose PK study, female cynomolgus monkeys (*Macaca fascicularis*) received intravenous 0.3, 3, or 30 mg/kg pembrolizumab, and serum concentrations were determined by ELISA. For the toxicokinetic analyses included in the repeat-dose toxicity studies, serum pembrolizumab concentrations were determined using an ECL immunoassay. In both the ELISA and ECL assays, serum pembrolizumab concentrations were determined by ligand capture using human PD-1-Fc and antihuman kappa chain antibody for detection. For anti-pembrolizumab antibody detection (ADA), a bridging ECL method was used with biotinylated pembrolizumab as capture, ruthenylated pembrolizumab as detection, and affinity purified rabbit polyclonal anti-pembrolizumab as a positive control. To assess target engagement, an *ex vivo* whole blood assay was used to determine potentiation of IL2 secretion in PBMCs after SEB stimulation (described above).

Safety of pembrolizumab was evaluated in 1- and 6-month repeat-dose toxicity studies with a 4-month recovery period in cynomolgus monkeys. In the 1-month study, animals (6/sex/group) received 5 weekly intravenous doses of vehicle or pembrolizumab at 6, 40, or 200 mg/kg for total of five doses. Four animals/sex/group were euthanized during Week 5 whereas the remaining two animals/sex/group were euthanized during Week 23, after a 4-month treatment-free period. In this study, an assessment of target engagement was evaluated using the *ex vivo* IL2 SEB bioactivity assay (described above). In the 6-month study, animals (5/sex/group) received intravenous doses of vehicle or pembrolizumab at 6, 40, or 200 mg/kg once every other week for a total of 12 doses. Three animals/sex/group were designated for necropsy at the end of the 6-month dosing phase, and the remaining animals underwent necropsy following the 4-month treatment-free period. In both studies, in-life examinations included monitoring of food consumption, body weight, and clinical observations. Clinical pathology parameters (hematology, coagulation, serum chemistry, and urinalysis) were assessed periodically during the dosing phase on all animals. In addition, ophthalmic and electrocardiogram evaluations were performed at the end of dosing periods on all animals. Postmortem examinations included organ weights, and macroscopic and microscopic evaluations of all major tissues.

Animal studies

Procedures involving the care and use of animals were reviewed and approved by the Institutional Animal Care and Use Committee at Research Laboratories of Merck & Co., Inc. and adhere to the US Public Health Service Policy on Humane Care and Use of Laboratory Animals. Toxicology studies were conducted in compliance with

Table 1. Pembrolizumab binds with high affinity to human and cynomolgus monkey PD-1 and blocks the binding of both PD-L1 and PD-L2 to PD-1.

Assay	Target	K_D average (pmol/L)	K_D SD (pmol/L)	Number of tests
Binding to human PD-1				
Solid phase interferometry (Octet)	Human PD-1-Fc	29	ND	1
Surface plasmon resonance (Biacore)	Human PD-1-Fc	120, 130	ND	2
Surface plasmon resonance (Biacore)	Human PD-1-Fc	51	15	16[a]
Kinetic exclusion assay (KinExA)	Human PD-1-Fc	1.1	0.4	16[a]
Binding to cynomolgus monkey PD-1				
Solid-phase interferometry (Octet)	Cynomolgus monkey PD-1-Fc	118	ND	1
Surface plasmon resonance (Biacore)	Cynomolgus monkey PD-1-Fc	450, 470	ND	2
Competition with ligand binding to by PD-1 FMAT[b]				
	PD-L1 IC_{50} (pmol/L) (±SEM)		*PD-L2 IC_{50} (pmol/L) (±SEM)*	
Human	625 (130)		695 (360)	
Cynomolgus monkey	721 (150)		762 (200)	

Abbreviation: ND, not determined.
[a]The same 16 batches of pembrolizumab were evaluated using the Biacore and KinExA assays for binding to human PD-1-Fc.
[b]The results presented are an average of three independent experiments using an FMAT method where human or cynomolgus monkey PD-1 is expressed on Chinese hamster ovary cells.

Good Laboratory Practice at the Safety Evaluation Center, Schering Plough Research Institute (part of Merck & Co., Inc.), Merck & Co., Inc., and Charles River Laboratories.

Statistical analyses

Statistical analyses for data presented in **Table 1**, **Fig. 2** all panels, and **Fig. 3** panel A were performed using Prism software (GraphPad). Arithmetic means are reported in **Table 2**; PK analyses were performed using WinNonlin. Analyses for **Fig. 3** panel B were performed using NONMEM software.

Results

Analysis of pembrolizumab binding and inhibition of ligand binding

Following immunization of mice and short-term B-cell culture (24), B-cell clones were identified producing antibodies that bind and block human PD-1. After immortalization and further characterization, clone hPD1.09A was humanized by CDR grafting. Pembrolizumab, the final humanized antibody construct of hPD-1.09A, was generated on a human IgG4/kappa isotype with the stabilizing Adair mutation (25) S228P sequence alteration, where serine 228 (EU index) was converted to proline.

Pembrolizumab bound human PD-1 with an affinity ranging from 1.1 to 130 pmol/L in studies using solid-phase interferometry, surface plasmon resonance, or kinetic exclusion (**Table 1**). The K_D for binding of pembrolizumab to human PD-1 resulting from the Octet experiment was 29 pmol/L. The Biacore and KinExA studies involved the same 16 batches. Most batches had a K_D value assessed by Biacore of about 50 pmol/L, whereas the K_D values obtained by KinExA range from 0.4 to 1.9 pmol/L.

Pembrolizumab bound to cynomolgus monkey PD-1 with a similar K_D of 118 to 470 pmol/L. Pembrolizumab inhibited the binding of human PD-L1 and PD-L2 to human PD-1 and the binding of cynomolgus monkey PD-L1 and PD-L2 to cynomolgus monkey PD-1 (**Table 1**). Pembrolizumab did not bind to mouse PD-1, or to immunoglobulin superfamily members human CD28, human CTLA-4, or human ICOS (see Supplementary Fig. S1).

Pembrolizumab displays a distinct interaction site with PD-1

NMR was used to further characterize the PD-1/pembrolizumab Fab interactions (**Fig. 1A–D**). The hPD-1/hPD-L1 complex x-ray crystal structure (PDB code 4zqk; ref. 26) was used as a point of reference because this is the exact interaction that is being disrupted by antibody binding. The structure identifies residues in the C′CFG β strands of PD-1 that interact with PD-L1. In addition, the CC′ loop undergoes rearrangement upon PD-L1 binding. In all, 21 PD-1 residues are involved at the complex interface that spans 1970 Å^2. A flexible C′D loop is observed in the hPD-1/hPD-L1 structure that is disordered in the sPD-1 structure.

The x-ray crystal structure of PD-1/pembrolizumab Fab (PDB code 5ggs; ref. 27) revealed a widespread structural epitope consisting of atoms from PD-1 BC loop residues T59-F63; C strand residues V64, N66, and Y68; C′ strand residues Q75-K78 and A81; C′D loop residues P83 and D85-G90; F strand residue I126; FG loop residues L128-A132; G strand residue I134. The regions highlighted in blue in **Fig. 1** include 27 residues and cover 2081 Å^2 corresponding to 30% of the protein surface.

NMR binding studies were used to detect specific PD-1 residues affected by pembrolizumab Fab binding (**Fig. 1**) and were mapped to the existing structure (PDB code 5ggs). In these studies, the ^{15}N-edited HSQC data from ^{15}N-labeled sPD-1 was compared with data collected from a complex of ^{15}N-labeled PD-1 bound to unlabeled pembrolizumab Fab. These experiments collected data only from PD-1 residues; changes that occurred upon Fab binding can be identified for each residue. From NMR spectroscopy, residues that experienced the largest changes were: PD-1 BC loop residues N58, S62; C strand residues N66 and Y68, C′ strand residues D77, K78, and L79; C′D loop residues F82, D85, R86, Q88, G90, Q91, D92, F95; FG loop residues A129, A132, Q133; G strand residues I134 and S137. Other regions that were affected included D strand residue V97; F strand residues L122, G124, and I126 that were likely affected by the disruption of the FG loop. The regions highlighted in green (**Fig. 1**) include 24 residues that cover 1337 Å^2, corresponding to 19% of the protein surface. Rearrangement of the C′D loop and F strand residues L122-C123-G124 due to PD-L1 binding to sPD-1 was previously noted (28).

NMR studies were also used to determine the specific PD-1 residues affected by binding of a nivolumab Fab (**Fig. 1E–G**). In these studies, the ^{15}N-edited HSQC data from ^{15}N-labeled sPD-1 was compared with data collected from a complex of ^{15}N-labeled PD-1 bound to unlabeled nivolumab Fab. Relatively few peaks were shifted in the complex spectra consistent with a focused epitope. The 13 residues that were

Table 2. Summary of PK parameters following a single intravenous dose of pembrolizumab and TK parameters following weekly repeat intravenous dosing (1-month toxicology study) in female cynomolgus monkeys.

	PK parameters for single intravenous dose		
Dose (number of animals)	**0.3 mg/kg[a] (*N* = 3)**	**3 mg/kg[a] (*N* = 3)**	**30 mg/kg[a] (*N* = 3)**
Cmax (μg/mL)[b]	15.3 ± 4.3	117.7 ± 5.2	1,265 ± 73
$AUC_{0\text{-last}}$ (μg·day/mL)[c]	41.0 ± 2.9	700.0 ± 76.5	6,374 ± 767
CL (mL/day/kg)	5.7 ± 0.2	4.2 ± 0.4	3.7 ± 0.1
$t_{1/2}$ (days)	3.9 ± 0.7	5.9 ± 1.6	10.6 ± 0.4
V_{ss} (mL/kg)	30.9 ± 6.0	36.8 ± 4.6	54.8 ± 5.7
	TK parameters for weekly repeat intravenous dosing (1-month toxicology study)		
Dosing day (number of doses[d])	**Day 1 (1)**		**Day 28 (5)**
Dose (mg/kg)	6	40	200	6	40	200
C_{max} (μg/mL)	292	2,510	14,800	350	4,770	86,200
T_{max} (hour)[e]	1 (1–24)	1 (1–168)	1 (1–48)	2 (1–24)	2 (1–168)	3 (1–24)
$t_{1/2}$ (days)	ND	ND	ND	15.7	22.3	19.8
$AUC_{0\text{-7 days}}$ (μg·day/mL)	923	7,240	49,700	1,790	24,100	170,000
AUC R[c]	NA	NA	NA	1.78	3.12	5.58

Abbreviations: ADA, antidrug antibodies; $AUC_{0\text{-last}}$, area under the concentration curve from time zero to the last time point; CL, clearance; C_{max}, maximum concentration; hr, hours; NA, not applicable; ND, not determined; PK, pharmacokinetic; $t_{1/2}$, terminal half-life; TK, toxicokinetic; T_{max}, time to maximum concentration; V_{ss}, volume of distribution at steady state.

[a]All three monkeys in each dose group were included in the analysis.

[b]Values shown ± SEM.

[c]Because of ADA, sample concentrations that were less than 1 mg/L were excluded from the exposure calculation. Therefore, AUC0-last was different for different animals: the last time point for 3 monkeys in the 0.3 mg/kg group were 14, 7, and 14 days; for 3 mg/kg last three time points were 42, 28, and 14 days, and for 30 mg/kg last three time points were 28, 14, and 63 days.

[d]AUC ratio: $R = AUC_{(0\text{–}7\ days)}$ dosing interval 5 $AUC_{(0\text{–}7\ days)}$ dosing interval 1; mean calculated from *R* values from individual animals.

[e]Median (minimum to maximum).

most affected were N loop residues S27 and D29, BC loop residues N58 and S60 and FG loop residues A129, A132, and Q133. Other affected residues were not localized in loops; they included T36, S54, N64, H107, and Y121. When mapped to the PDB code 5wt9 crystal structure, the N-terminal BC and FG loops were spatially clustered together and, as a result, can be identified as the Fab binding location. The regions cover 711 $Å^2$, corresponding to 9% of the protein surface.

Single residue resolution of the NMR HSQC data allowed for the differentiation of nivolumab from pembrolizumab binding to PD-1 even without knowledge of sequence-specific assignments. Pembrolizumab and nivolumab demonstrated distinct binding interaction sites on PD-1 (**Fig. 1G**).

In vitro activity of pembrolizumab

Pembrolizumab enhanced SEB-induced production of IL2 (29) by 3- to 4-fold over SEB alone in an *ex vivo* assay on PBMCs from healthy human donors (22) as well as from patients with advanced metastatic melanoma (22) or prostate cancer (22), indicating that blood cells derived from healthy donors and patients with cancer contained T cells sensitive to modulation by pembrolizumab. Pembrolizumab activity was also confirmed in SEB-stimulated PBMC cultures from cynomolgus monkeys with similar enhancement of IL2 production (22).

To assess the influence of pembrolizumab on antigen-specific memory T-cell responses, a human T-cell recall assay using TT was conducted using PBMCs from volunteers who had received a TT booster vaccination within the previous year (22). Production of IFNγ was enhanced by PD-1 blockade using pembrolizumab in a dose-dependent manner (**Fig. 2A**), evidence that PD-1 blockade relieved PD-1/PD-L1/PD-L2 immune suppression and resulted in enhanced antigen-specific T cell IFNγ production.

Pembrolizumab ability to enhance IFNγ production in a T-cell clone co-culture assay was also assessed. T-cell clone BC4-49 expresses PD-1 and is susceptible to checkpoint inhibition, including inhibition of proliferation and IFNγ production when binding either PD-L1 or PD-L2 in the context of allo-antigen recognition. Using a JY transfected clone expressing high levels of PD-L1, coculture of T-cell clone BC4-49 with JY-PD-L1 cells resulted in low levels of IFNγ production. This was reversed by pembrolizumab in a dose-dependent manner (**Fig. 2B**).

The potential of pembrolizumab to induce IFNγ production in human primary tumors was evaluated in cultures of anti-CD3-stimulated primary tumor cell digests (30). In these experiments, NSCLC tumor specimens were treated with pembrolizumab or an isotype control antibody. A dose-dependent increase in IFNγ secretion with pembrolizumab treatment was observed (**Fig. 2C**).

Evaluation of cytokine release, ADCC, and CDC activity for pembrolizumab

In both the PBMC cytokine release assay with plate-bound antibodies and in solution in the whole blood assay, cytokine levels induced by pembrolizumab were low and comparable to those induced by trastuzumab, a therapeutic antibody with a safe clinical profile for cytokine release (see Supplementary Tables S1 and S2). PD-1 was saturated by pembrolizumab at 0.1 μg/mL on activated target human $CD4^+$ T cells. PD-1 expression was comparable to the levels observed on the activated target human $CD4^+$ T cells used in the CDC and ADCC assays. A concentration of pembrolizumab exceeding that needed for saturation of PD-1 was used. Pembrolizumab ADCC and CDC induction was comparable to the negative control, human IgG4 anti-PCSK9 antibody and mouse IgG2a isotype control antibody, whereas an anti-MHC class I positive control antibody induced robust cell killing (Supplementary Figs. S2 and S3).

Ex vivo analysis of pembrolizumab impact on antigen-specific T-cell recall response to viral antigens

The effect of treatment with pembrolizumab on overall T-cell response to viral infection was assessed *ex vivo* in the clinical trial

Table 3. Toxicological evaluation of pembrolizumab in cynomolgus monkey and calculation of systemic exposure multiples.

Species	Study duration	Dose levels (mg/kg/day)	$AUC_{0\text{-}tau}$ (μg·day/mL) dosing interval 5 or 11[a]	Exposure multiple	
				2.0 mg/kg[b,d]	10.0 mg/kg[c,d]
Cynomolgus monkey	1 month	6	1,790	2.5	0.5
		40	24,100	33	6.7
		200 (NOAEL)	170,000	236	47
	6 months	6	1,200	1.7	0.3
		40	13,417	19	3.7
		200 (NOAEL)	67,500	94	19

Abbreviations: EM, exposure multiple; NOAEL, no observed adverse effect level; Q2W, once every 2 weeks; Q3W, once every 3 weeks.
[a]Tau, 7 days in the 1-month study and data are from dosing interval 5 (study week 5); tau, 14 days in the 6-month study and data are from dosing interval 11 (study weeks 21–22).
[b]EM at predicted $AUC_{0\text{-}tau}$ of 721.5 μg·day/mL for the clinical dose of 2 mg/kg, Q3W.
[c]EM at predicted $AUC_{0\text{-}tau}$ of 3607.3 μg·day/mL for the clinical dose of 10 mg/kg, Q3W and Q2W. $AUC_{0\text{-}tau}$ is by definition independent of schedule and therefore the EMs for Q2W and Q3W are identical.
[d]Clinical AUC at steady state calculated from clearance as dose divided by clearance and normalized to 1 week. Clearance was determined by population PK modeling at 0.219 L/day.

KEYNOTE-001 on patients with solid tumors using a viral recall assay. PBMCs from 17 patients isolated prior to and after up to 4 weeks of treatment with pembrolizumab were stimulated with a pool of peptides of Epstein–Barr virus, cytomegalovirus, and influenza virus restricted to MHC class I molecules and assessed for IFNγ expression. There was no significant change in IFNγ production after pembrolizumab treatment using Wilcoxon-signed rank test (paired difference test), indicating no compromise of overall virus specific T-cell–mediated immune response (**Fig. 2D**).

Pharmacokinetics of pembrolizumab in cynomolgus monkeys

After administering single intravenous doses of pembrolizumab at 0.3, 3, or 30 mg/kg to cynomolgus monkeys, a slightly more than dose-proportional exposure between 0.3 and 3.0 mg/kg was observed, and approximately dose-proportional exposure was observed between 3.0 and 30 mg/kg (**Table 2**). Clearance and terminal half-life ($t_{1/2}$) appeared to be dose-dependent, with the higher dose groups exhibiting slower clearance and longer $t_{1/2}$, suggesting a possible involvement of target mediated clearance at the low dose. See Supplementary Table S3 for more detail.

Toxicological evaluation of pembrolizumab in cynomolgus monkeys

Pembrolizumab was well-tolerated in cynomolgus monkeys with a systemic exposure ($AUC_{0\text{-}7\ days}$) of up to approximately 170,000 μg·day/mL with weekly dosing over the course of a 1-month study, and with a systemic exposure ($AUC_{0\text{-}14\ days}$) of up to approximately 67,500 μg·day/mL with biweekly dosing over the course of a 6-month study (**Tables 2** and **3**).

In both the 1-month and the 6-month studies, no adverse findings were observed in any antemortem monitoring. At terminal evaluations (end of dosing and end of treatment-free period necropsy), there were no pembrolizumab-related organ weight, macroscopic, or histopathologic findings. Most histomorphologic changes observed in a few scattered organs/tissues generally consisted of small, focal, mononuclear cellular infiltration, composed primarily of lymphocytes and/or histiocytes, without parenchymal organ tissue disruption or degeneration, similar in character and magnitude to spontaneous changes commonly observed in cynomolgus monkeys (31, 32). On the basis of these results, the no-observed-adverse-effect-level (NOAEL) in both monkey studies was determined as the highest tested dose of 200 mg/kg.

In both the PK and 1-month toxicity study, monkeys' biological response to pembrolizumab was confirmed using *ex vivo* potentiation of IL2 secretion in peripheral blood cells following stimulation with SEB (**Fig. 3A**). Prior to dosing, *ex vivo* addition of pembrolizumab and SEB to blood potentiated IL2 production 2- to 3-fold. However, the potentiation of IL2 production was not observed in blood collected from pembrolizumab-dosed animals, indicating prior PD-1 engagement by pembrolizumab. Engagement was observed across all dose levels in both the PK and toxicology study immediately following dose administration on both the first and last day of dosing, and returned to baseline following antibody clearance in a dose-dependent manner (**Fig. 3B**). During the 4-month postdose period in the 1 month toxicology study, in the 6 and 40 mg/kg dose groups target engagement activity returned to prestudy levels around 1 and 2 months, respectively, whereas in the 200 mg/kg group engagement was still evident at 4 months, indicating full PD-1 engagement for the entire duration of the toxicology study.

Discussion

Pembrolizumab is a humanized IgG4 (S228P) anti-PD-1 antibody that binds to human and cynomolgus monkey PD-1 with high affinity. Although there is no international standard for determining affinity, three different methods show that pembrolizumab binds human PD-1 with picomolar affinity. In addition, pembrolizumab potently blocks both PD-1 ligands PD-L1 and PD-L2 from binding to PD-1.

The binding interaction sites between PD-1 and either PD-L1 or PD-L2 are known (26–28, 33–37). Structural studies have shown that the pembrolizumab binding interaction site on PD-1 overlaps with the PD-L1 binding site (27, 36–38) and involves the C′D and FG loops of PD-1. Structural, biochemical, and biophysical methods have been used to better understand the interactions of PD-1 with pembrolizumab and another anti-PD-1 therapeutic, nivolumab (36, 38–40). The pembrolizumab binding interaction site with PD-1 is distinct from that of nivolumab (36, 38–40). High-resolution x-ray crystal structures and solution NMR studies reveal that pembrolizumab binding affects many of the same PD-1 residues that directly interact with PD-L1 and PD-L2, directly blocking the binding of the endogenous ligands (41). In contrast, PD-1-nivolumab interactions primarily affect flexible PD-1 N-terminal residues (39, 41). Deletion of the PD-1 N-terminus abolished nivolumab binding whereas pembrolizumab binding was unaffected.

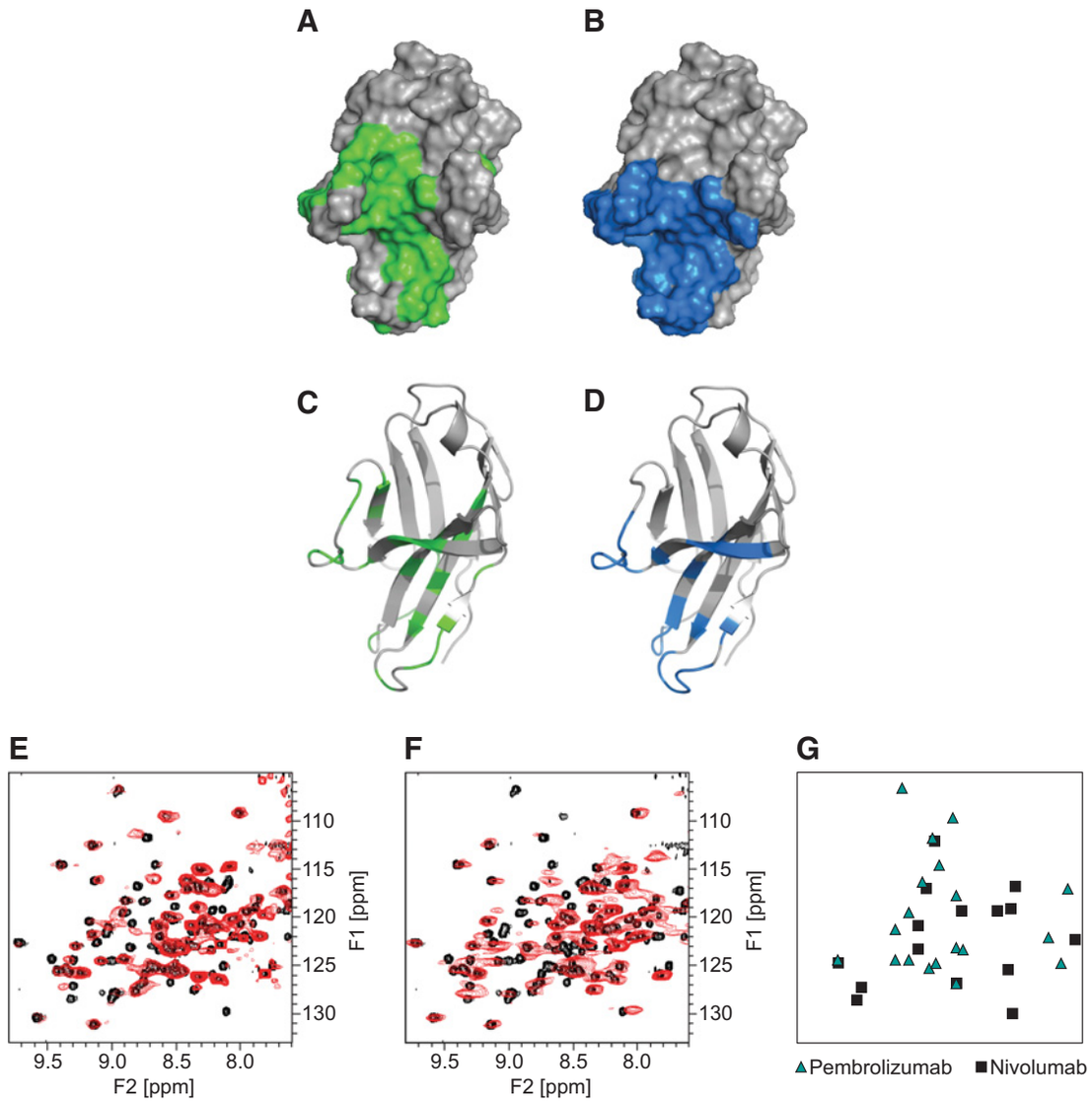

Figure 1.

Differentiation of pembrolizumab and nivolumab binding site on PD-1. The pembrolizumab interaction site on PD-1 is depicted from NMR spectroscopy data (**A** and **C**), and from X-ray crystallography data (**B** and **D**). The identification of PD-1 residues that are affected by Fab binding is achieved by comparing ^{1}H and ^{15}N sPD-1 peak positions in the apo-PD-1 and PD-1/Fab complex data sets in **E–G**. Residues that are affected by pembrolizumab are colored green (**A** and **C**) or blue (**B** and **D**) and mapped to the surface of PD-1. PD-1 residues that are unaffected are shown in gray. The PD-1 residues shown are based on PD-1 coordinates from the PD-1/pembrolizumab Fab complex (PDB code 5ggs). The panels highlight specific residues that are affected by Fab binding and demonstrate the alignment between the different methods. **E** shows an overlay of ^{15}N-HSQC NMR data for the PD-1/nivolumab Fab complex (red) and apo-PD-1 (black), whereas **F** shows an overlay of ^{15}N-HSQC NMR data for the PD-1/pembrolizumab Fab complex (red) and apo-PD-1 (black). In **G,** green triangles are placed at the ^{1}H-^{15}N peak positions of apo-PD-1 residues that are affected by pembrolizumab binding. Black rectangles are placed at apo-PD-1 peak positions that are affected by nivolumab binding.

Lepir and colleagues (38) hypothesized that the affinity strength of pembrolizumab is mainly due to the HCDR3 loop, which binds both the C′D and FG loops of PD-1. Na and colleagues (37) structurally superimposed the human PD-1/pembrolizumab Fab complex and their model of the human PD-1/human PD-L2 complex and concluded that the binding interaction sites overlap in regions similar to those observed for pembrolizumab and PD-L1.

The ability of pembrolizumab to block binding of both PD-L1 and PD-L2 to PD-1 is an important feature of its clinical mechanism of action. The signaling functions of PD-1/PD-L1 and PD-1/PD-L2 overlap partially but not completely (42–44). The importance of being able to block not just PD-L1 but also PD-L2 is highlighted by the fact that tumors and their microenvironments may express either PD-L1, PD-L2, or both (44, 45). A preclinical mouse study (43) suggests that although PD-1/PD-L1 suppression is the primary mechanism for cancer immune evasion, PD-L2 upregulation may be a compensatory mechanism once PD-L1 function is nullified.

Pembrolizumab demonstrated functional activity by reversing PD-1 immune-mediated suppression in human T-cell SEB stimulation, $CD4^{+}$/HLA-DR alloantigen-specific T-cell clone co-culture,

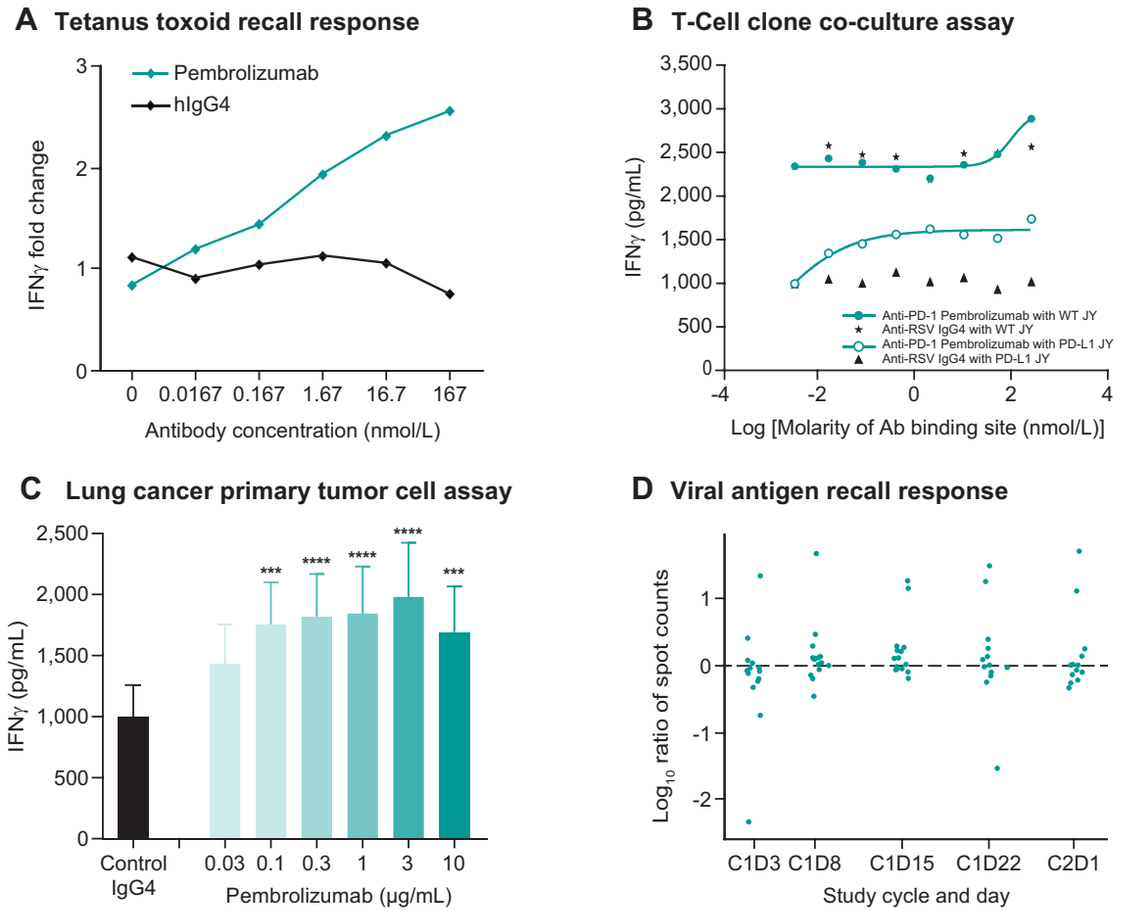

Figure 2.

Pembrolizumab enhances T-cell activation *in vitro*. In **A,** TT-induced production of IFNγ from PBMCs (**A**). To determine IFNγ fold-change, the cytokine level in the presence of antibody is compared with the cytokine level in the absence of antibody. Pembrolizumab is indicated by the green diamond whereas the control is shown in black. In **B,** IFNγ production from HLA-DR alloreactive human $CD4^+$ T-cell clones. In the coculture of T-cell clone BC4-49 with JY-PD-L1 IFNγ production was inhibited, with pembrolizumab as the open green circles and the control as black triangles. In **C,** IFNγ secretion in cultures of anti-CD3-stimulated primary NSCLC tumor cell digests. IFNγ secretion is a marker for activated $CD3^+$ tumor infiltrating lymphocytes. In **D,** 17 patients were tested with IFNγ ELISPOT assay. Blood samples were collected at pretreatment and post-pembrolizumab treatment time points as indicated, cycle 1 day 3 (C1D3), cycle 1 day 8 (C1D8), cycle 1 day 22 (C1D22), and cycle 2 day 1 (C2D1). PBMC were stimulated in triplicate with an MHC class I restricted viral peptide pool from Epstein–Barr virus, cytomegalovirus, and influenza virus (CEF-32) and tested with IFNγ ELISPOT assay. Line indicates mean of IFNγ spots from 400,000 mononuclear cells.

and primary tumor cell histoculture assays by inducing or enhancing production of IL2 and IFNγ, a marker of tumor-infiltrating lymphocytes (30). Although pembrolizumab allows stimulated T cells to become active, it does so in an antigen-specific manner as evidenced by the $CD4^+$/HLA-DR alloantigen-specific T-cell clone, TT recall response, and viral antigen response results.

The pembrolizumab IgG4 framework heavy chain is constructed using an S228P mutation, which prevents Fab arm exchange with endogenous IgG4 molecules (46). Consistent with its IgG4 framework, pembrolizumab does not mediate effector functions, as assessed by ADCC and CDC. Nor does pembrolizumab directly cause cytokine release, as demonstrated using human PBMC and whole blood assays.

Pembrolizumab was well-tolerated up to 200 mg/kg either once weekly for 1 month or once every 2 weeks for 6 months in cynomolgus monkeys, where dose dependent and significant systemic exposure was demonstrated. Most histopathology observations in these studies were limited to incidental histomorphologic changes observed in scattered organs/tissues in individual monkeys that were similar in character to spontaneously occurring background findings in cynomolgus monkeys (31, 32). Although potential exacerbation of spontaneous tissue changes by the treatment with pembrolizumab cannot be ruled out, the findings were nonadverse to the study animals. The safety profile of pembrolizumab in monkeys appears to be similar to nivolumab although the study designs for the two antibodies were different in dose level, dose frequency, and duration of treatment. The nivolumab toxicology study (23) in cynomolgus monkeys with twice weekly intravenous administration of 10 or 50 mg/kg over a 3-month period (27 total doses) demonstrated the highest well-tolerated dose was 50 mg/kg. The only toxicology-related finding was a reversible decrease (by 28%) in serum triiodothyronine (T3) hormone in females treated with 50 mg/kg at week 13, whereas thyroxine (T4) and thyroid-

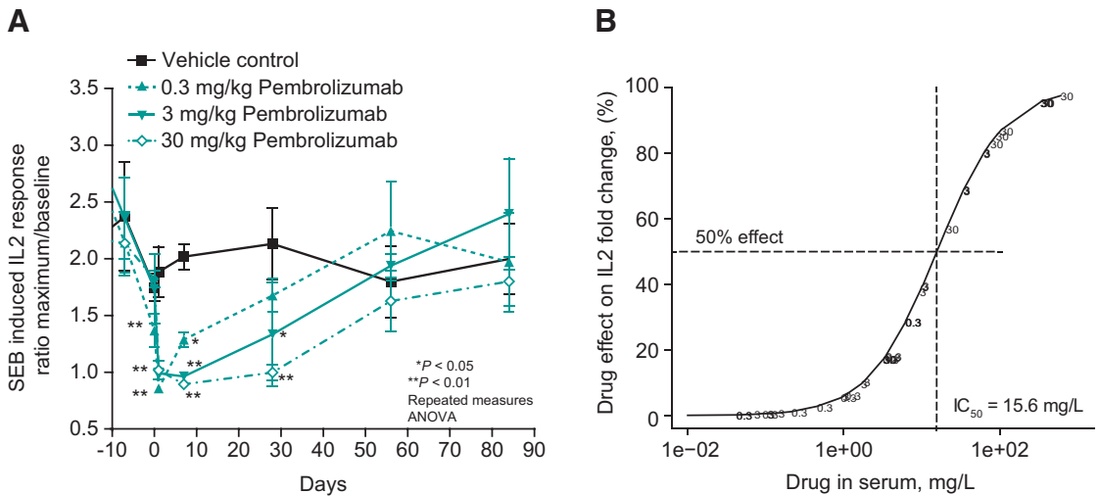

Figure 3.

Dose- and time-dependent *ex vivo* modulation of SEB-induced IL2 production by cynomolgus monkey blood cells after administration of pembrolizumab. PD-1 target engagement was evaluated *ex vivo* by assessing potentiation of IL2 secretion in peripheral blood cells following stimulation with SEB. To compare values between different time points and assays, IL2 level fold change was calculated. ANOVA repeated measures was used for statistical analysis. **A** shows the *ex vivo* SEB assay IL2 production fold-changes for each dose group over the course of the study. **B** shows the pharmacodynamic relationship between the target engagement assay results (IL2 fold-change in percentage) and the concentration of pembrolizumab in serum.

stimulating hormone (TSH) levels were unchanged. The significance of this finding was not discussed and no other findings from the nivolumab toxicology study were reported (23).

Pembrolizumab has demonstrated efficacy in multiple cancers and is currently approved for treatment of more than 15 different indications (47). Clinical studies continue to examine the effectiveness of pembrolizumab alone or in combination with other agents in multiple cancers.

Disclosure of Potential Conflicts of Interest

All authors are current or former employees of Merck Sharp & Dohme Corp., a subsidiary of Merck & Co., Inc., and may own stock/stock options in Merck & Co., Inc. J. Dulos has a patent W02008156712A1, relevant to work. H. van Eenennaam has stock from Aduro, Inc., outside the submitted work. In addition, H. van Eenennaam has a patent WO/2008/156712 issued, relevant to work. Gregory J. Carven is a current employee of Scholar Rock and is a named inventor on patents and patent applications related to pembrolizumab.

Authors' Contributions

Conception and design: L. Fayadat-Dilman, M. Hsieh, S. Li, S. Sadekova, M.A. McCoy, D. Herzyk, F.M. Poulet, J. Dulos, C.L. Andrews, R. de Waal Malefyt, J. Lee, H. van Eenennaam, A. Willingham, Y. Yu, M. Streuli, G.J. Carven, A. van Elsas

Development of methodology: L. Fayadat-Dilman, M. Hsieh, S. Li, M.A. McCoy, F.M. Poulet, J. Dulos, C.L. Andrews, G. Ayanoglu, C. Cullen, R. de Waal Malefyt, J. Lee, S. Sadekova, H. van Eenennaam, A. Willingham, Y. Yu, M. Streuli, G.J. Carven, A. van Elsas

Acquisition of data (provided animals, acquired and managed patients, provided facilities, etc.): C. Cullen, M.A. McCoy, F.M. Poulet, J. Dulos, S.P. Kang, G. Ayanoglu, J. Lee, S. Li, D. Malashock, G. Soder, Y. Yu, G.J. Carven

Analysis and interpretation of data (e.g., statistical analysis, biostatistics, computational analysis): D. Herzyk, S.P. Kang, R.A Kastelein, S. Sadekova, A. van Elsas, B. Hutchins, G.C. Starling, M.A. McCoy, F.M. Poulet, J. Dulos, L. Liu, L. Fayadat-Dilman, C.L. Andrews, C. Cullen, R. de Waal Malefyt, S. Le Saux, S. Li, D. Malashock, H. van Eenennaam, A. Willingham, Y. Yu, M. Streuli, G.J. Carven

Writing, review, and/or revision of the manuscript: B. Hutchins, G.C. Starling, M.A. McCoy, D. Herzyk, F.M. Poulet, J. Dulos, L. Liu, S.P. Kang, L. Fayadat-Dilman, M. Hsieh, C.L. Andrews, G. Ayanoglu, C. Cullen, R. de Waal Malefyt, R.A. Kastelein, S. Le Saux, J. Lee, S. Li, D. Malashock, S. Sadekova, G. Soder, H. van Eenennaam, A. Willingham, Y. Yu, M. Streuli, G.J. Carven, A. van Elsas

Administrative, technical, or material support (i.e., reporting or organizing data, constructing databases): J. Dulos

Study supervision: J. Dulos, C. Cullen, R.A. Kastelein, S. Sadekova, H. van Eenennaam, M. Streuli, A. van Elsas

Other (data verification): B. Hutchins

Other (drafting of the first draft): B. Hutchins, G.C. Starling, M.A. McCoy, D. Herzyk, L. Liu, R. de Waal Malefyt

Acknowledgments

This study was funded by Merck Sharp & Dohme Corp., a subsidiary of Merck & Co., Inc. The authors wish to acknowledge the following individuals (all of Merck Sharp & Dohme Corp., a subsidiary of Merck & Co., Inc., Kenilworth, NJ USA): Karen Kolz, Yifan Song, Dong-Hun Lee for collection of data; Corey Strickland for structural biology input; Jayanthi Wolf for supervision of research and input on study design and data interpretation; Lauren Nardini for collection of data and bioanalytical development, validation and sample analysis; Shree Bhagwat, David Sanden, and Shawn Foti for technical help and collection of data; Michael Judo for collection of data for specificity; Saraswathi Naravula and Kasia Marullo for technical help and collection of data; Wiebe Olijve and Ton Adang for supervision of research; Amy Levonas for technical help, writing assistance, and administrative or logistic support; Sheila Erespe for submission assistance; Narendra Kishnani for PK/TK analysis; Cathelijne Kloks for collection of data, supervision of research, and development and validation of pharmacokinetic and immunogenicity assays for (pre)clinical studies of pembrolizumab.

The costs of publication of this article were defrayed in part by the payment of page charges. This article must therefore be hereby marked *advertisement* in accordance with 18 U.S.C. Section 1734 solely to indicate this fact.

Received August 15, 2019; revised December 3, 2019; accepted March 11, 2020; published first March 30, 2020.

References

1. Sharma P, Hu-Lieskovan S, Wargo JA, Ribas A. Primary, adaptive, and acquired resistance to cancer immunotherapy. Cell 2017;168:703–23.
2. Sharma P, Allison JP. The future of immune checkpoint therapy. Science 2015; 348:56–61.
3. Simon S, Labarriere N. PD-1 expression on tumor-specific T cells: friend or foe for immunotherapy? Oncoimmunology 2017;7:e1364828.
4. Ishida Y, Agata Y, Shibahara K, Honjo T. Induced expression of PD-1, a novel member of the immunoglobulin gene superfamily, upon programmed cell death. EMBO J 1992;11:3887–95.
5. Keir ME, Butte MJ, Freeman GJ, Sharpe AH. PD-1 and its ligands in tolerance and immunity. Annu Rev Immunol 2008;26:677–704.
6. Hui E, Cheung J, Zhu J, Su X, Taylor MJ, Wallweber HA, et al. T cell costimulatory receptor CD28 is a primary target for PD-1-mediated inhibition. Science 2017;355:1428–33.
7. Kamphorst AO, Wieland A, Nasti T, Yang S, Zhang R, Barber DL, et al. Rescue of exhausted CD8 T cells by PD-1-targeted therapies is CD28-dependent. Science. 2017;355:1423–7.
8. Yokosuka T, Takamatsu M, Kobayashi-Imanishi W, Hashimoto-Tane A, Azuma M, Saito T. Programmed cell death 1 forms negative costimulatory microclusters that directly inhibit T cell receptor signaling by recruiting phosphatase SHP2. J Exp Med 2012;209:1201–17.
9. Arasanze H, Gato-Cañas M, Zuazo M, Ibañez-Vea M, Breckpot K, Kochan G, et al. PD1 signal transduction pathways in T cells. Oncotarget 2017;8:51936–45.
10. Zou W, Chen L.Inhibitory B7-family molecules in the tumour microenvironment. Nat Rev Immunol 2008;8:467–77.
11. Kuang DM, Zhao Q, Peng C, Xu J, Zhang JP, Wu C, et al. Activated monocytes in peritumoral stroma of hepatocellular carcinoma foster immune privilege and disease progression through PD-L1. J Exp Med 2009;206xs:1327–37.
12. Hino R, Kabashima K, Kato Y, Yagi H, Nakamura M, Honjo T, et al. Tumor cell expression of programmed cell death-1 ligand 1 is a prognostic factor for malignant melanoma. Cancer 2010;116:1757–66.
13. Massi D, Brusa D, Merelli B, Ciano M, Audrito V, Serra S, et al. PD-L1 marks a subset of melanomas with a shorter overall survival and distinct genetic and morphological characteristics. Ann Oncol 2014;25:2433–42.
14. Taube JM, Klein A, Brahmer JR, Xu H, Pan X, Kim JH, et al. Association of PD-1, PD-1 ligands, and other features of the tumor immune microenvironment with response to anti-PD-1 therapy. Clin Cancer Res 2014;20:5064–74.
15. Chen YB, Mu CY, Huang JA. Clinical significance of programmed death-1 ligand-1 expression in patients with non-small cell lung cancer: a 5-year-follow-up study. Tumori 2012;98:751–5.
16. Boland JM, Kwon ED, Harrington SM, Wampfler JA, Tang H, Yang P, et al. Tumor B7-H1 and B7-H3 expression in squamous cell carcinoma of the lung. Clin Lung Cancer 2013;14:157–63.
17. Yang CY, Lin MW, Chang YL, Wu CT, Yang PC. Programmed cell death-ligand 1 expression in surgically resected stage I pulmonary adenocarcinoma and its correlation with driver mutations and clinical outcomes. Eur J Cancer 2014;50: 1361–9.
18. Velcheti V, Schalper KA, Carvajal DE, Anagnostou VK, Syrigos KN, Sznol M, et al. Programmed death ligand-1 expression in non-small cell lung cancer. Lab Invest 2014;94:107–16.
19. Zhang Y, Wang L, Li Y, Pan Y, Wang R, Hu H, et al. Protein expression of programmed death 1 ligand 1 and ligand 2 independently predict poor prognosis in surgically resected lung adenocarcinoma. Onco Targets Ther 2014;7:567–73.
20. Iwai Y, Ishida M, Tanaka Y, Okazaki T, Honjo T, Minato N. Involvement of PD-L1 on tumor cells in the escape from host immune system and tumor immunotherapy by PD-L1 blockade. Proc Natl Acad Sci U S A 2002;99:12293–7.
21. Lee W, Tonelli Markley JL. NMRFAM-SPARKY: enhanced software for biomolecular NMR spectroscopy. Bioinformatics 2015;31:1325–7.
22. Dulos J, Carven GJ, van Boxtel SJ, Evers S, Driesen-Engels LJA, Hobo W, et al. PD-1 blockade augments Th1 and Th17 and suppresses Th2 responses in peripheral blood from patients with prostate and advanced melanoma cancer. J Immunother. 2012;35:169–178.
23. Wang C, Thudium KB, Han M, Wang X-T, Huang H, Feingersh D, et al. In vitro characterization of the anti-PD-1 antibody nivolumab, BMS-936558, and in vivo toxicology in non-human primates. Cancer Immunol Res 2014;2:846–56.
24. Steenbakkers PG, Boots AM, Rijnders AW. Generation and functional characterization of anti-clonotype antibodies to human T-cell receptors. J Immunol Methods 1997;210:51–64.
25. Angal S, King DJ, Bodmer MW, Turner A, Lawson AD, Roberts G, et al. A single amino acid substitution abolishes the heterogeneity of chimeric mouse/human (IgG4) antibody. Mol Immunol 1993;30:105–8.
26. Berman H, Henrick K, Nakamura H. Announcing the worldwide protein data bank. Nat Struct Biol 2003;10:980.
27. Scapin G, Yang X, Prosise WW, McCoy M, Reichert P, Johnston JM, et al. Structure of full-length human anti-PD1 therapeutic IgG4 antibody pembrolizumab. Nat Struct Mol Biol 2015;22:953–8.
28. Zak KM, Przemyslaw G, Magiera K, Dömling A, Dubin G, Holak TA. Structural biology of the immune checkpoint receptor PD-1 and its ligands PD-L1/PD-L2. Structure 2017;25:1163–74.
29. Chikuma S, Terawaki S, Hayashi T, Nabeshima R, Yoshida T, Shibayama S, et al. PD-1-mediated suppression of IL-2 production induces CD8+ T cell energy? in vivo. J Immunol 2009;182:6682–9.
30. Hellström I, Ledbetter JA, Scholler N, Yang Y, Ye Z, Goodman G, et al. CD3-mediated activation of tumor-reactive lymphocytes from patients with advanced cancer. Proc Natl Acad Sci U S A. 2001;98;6783–8.
31. Sato J, Doi T, Kanno T, Wako Y, Tsuchitani M, Narama I. Histopathology of incidental findings in cynomolgus monkeys (macaca fascicularis) used in toxicity studies. J Toxicol Pathol 2012;25:63–101.
32. Chamanza R, Marxfeld HA, Blanco AI, Naylor SW, Bradley AE. Incidences and range of spontaneous findings in control cynomolgus monkeys (Macaca fascicularis) used in toxicity studies. Toxicol Pathol 2010;38:642–57.
33. Lin DY, Tanaka Y, Iwasaki M, Gittis AG, Su HP, Mikami B, et al. The PD-1/PD-L1 complex resembles the antigen-binding Fv domains of antibodies and T cell receptors. Proc Natl Acad Sci U S A 2008;105:3011–6.
34. Zak KM, Kitel R, Przetocka S, Golik P, Guzik K, Musielak B, et al. Structure of the complex of human programmed death 1, PD-1, and its ligand pd-l1. Structure 2015;23:2341–8.
35. Lázár-Molnár E, Yan Q, Cao E, Ramagopal U, Nathenson SG, Almo SC. Crystal structure of the complex between programmed death-1 (PD-1) and its ligand PD-L2. Proc Natl Acad Sci U S A 2008;105:10483–8.
36. Lee JY, Lee HT, Shin W, Chae J, Choi J, Kim SH, et al. Structural basis of checkpoint blockade by monoclonal antibodies in cancer immunotherapy. Nat Commun 2016;7:13354.
37. Na Z, Yeo SP, Bharath SR, Bowler MW, Balkç E, Wang CI, et al. Structural basis for blocking PD-1-mediated immune suppression by therapeutic antibody pembrolizumab. Cell Res 2017;17:147–50.
38. Lepir T, Zaghouani M, Roche SP, Li YY, Suarez M, Irias MJ, et al. Nivolumab to pembrolizumab switch induced a durable melanoma response. Medicine (Baltimore). 2019;98:e13804.
39. Tan S, Zhang H, Chai Y, Song H, Tong Z, Wang Q, et al. An unexpected N-loop in PD-1 dominates binding by nivolumab. Nat Commun 2017;8:14369.
40. Tan S, Liu K, Chai Y, Zhang CW, Gao S, Gao GF, et al. Distinct PD-L1 binding characteristics of therapeutic monoclonal antibody durvalumab. Protein Cell 2018;9:135–9.
41. Lee HT, Lee SH, Heo Y-S. Molecular interactions of antibody drugs targeting PD-1, PD-L1, and CTLA-4 in immuno-oncology. Molecules 2019;24:1190.
42. Rozali EN, Hato SV, Robinson BW, Lake RA, Lesterhuis WJ. Programmed death ligand 2 in cancer-induced immune suppression. Clin Dev Immunol 2012;2012: 656340.
43. Umezu D, Okada N, Sakoda Y, Adachi K, Ojima T, Yamaue H, et al. Inhibitory functions of PD-L1 and PD-L2 in the regulation of anti-tumor immunity in murine tumor microenvironment. Cancer Immunol Immunother 2019;68:201–11.
44. Yearley JH, Gibson C, Yu N, Moon C, Murphy E, Juco J, et al. PD-L2 expression in human tumors: relevance to anti-PD-1 therapy in cancer. Clin Cancer Res 2017;23:3158–67.
45. Danilova L, Wang H, Sunshine J, Kaunitz GJ, Cottrell TR, Xu H, et al. Association of PD-1/PD-L axis expression with cytolytic activity, mutational load, and prognosis in melanoma and other solid tumors. Proc Natl Acad Sci U S A 2016;113:E7769–77.
46. Yang X, Wang F, Zhang Y, Wang L, Antonenko S, Zhang S, et al. Comprehensive analysis of the therapeutic IgG4 antibody pembrolizumab: hinge modification blocks half molecule exchange in vitro and in vivo. J Pharm Sci 2015;104:4002–14.
47. Keytruda (pembrolizumab) [prescribing information]. Whitehouse Station, NJ: Merck & Co., Inc; 2019.